Interannual-to-decadal variability of North Atlantic air-sea CO2 fluxes

Stéphane Raynaud, James C. Orr, Olivier Aumont, Keith B. Rodgers, Pascal Yiou

Ocean Sci., 2, 43–60, 2006
www.ocean-sci.net/2/43/2006/

Ocean Science

Interannual-to-decadal variability of North Atlantic air-sea CO_2 fluxes

S. Raynaud[1], J. C. Orr[1], O. Aumont[2], K. B. Rodgers[2,*], and P. Yiou[1]

[1]LSCE/IPSL, Laboratoire des Sciences du Climat et de l'Environnement, CEA-CNRS-UVSQ, Gif-sur-Yvette, France
[2]LOCEAN/IPSL, Laboratoire d'Océanographie et du Climat: Expérimentation et Approches Numériques, CNRS-IRD-UPMC, Paris, France
[*]now at: Atmospheric and Oceanic Sciences (AOS) Program, Princeton University, Princeton, USA

Abstract. The magnitude of the interannual variability of North Atlantic air-sea CO_2 fluxes remains uncertain. Interannual extremes simulated by atmospheric inverse approaches are typically about $\pm 0.3\,\mathrm{Pg\,C\,yr^{-1}}$, whereas those from ocean models are less than $\pm 0.1\,\mathrm{Pg\,C\,yr^{-1}}$. Thus variability in the North Atlantic is either about 60% or less than 20% of the global variability of about $\pm 0.5\,\mathrm{Pg\,C\,yr^{-1}}$ (as estimated by both approaches). Here we explore spatiotemporal variability within the North Atlantic basin of one ocean model in order to more fully describe potential counteracting trends in different regions that may explain why basin-wide variability is small relative to global-scale variability. Typical atmospheric inverse approaches separate the North Atlantic into at most a few regions and thus cannot properly simulate such counteracting effects. For this study, two simulations were made with a biogeochemical model coupled to a global ocean general circulation model (OGCM), which itself was forced by 55-year NCEP reanalysis fields. In the first simulation, atmospheric CO_2 was maintained at the preindustrial level (278 ppmv); in the second simulation, atmospheric CO_2 followed the observed increase. Simulated air-sea CO_2 fluxes and associated variables were then analysed with a statistical tool known as multichannel singular spectrum analysis (MSSA). We found that the subtropical gyre is not the largest contributor to the overall, basin-wide variability, in contrast to previous suggestions. The subpolar gyre and the inter-gyre region (the transition area between subpolar and subtropical gyres) also contribute with multipolar anomalies at multiple frequencies: these tend to cancel one another in terms of the basin-wide air-sea CO_2 flux. We found a strong correlation between the air-sea CO_2 fluxes and the North Atlantic Oscillation (NAO), but only if one takes into account time lags as does MSSA (maximum r=0.64 for lags between 1 and 3 years). The effect of increasing atmospheric CO_2 (the anthropogenic perturbation) on total variability was negligible at interannual time scales, whereas at the decadal (13-year) time scale, it increased variability by 30%.

Correspondence to: S. Raynaud
(stephane.raynaud@cea.fr)

1 Introduction

Inverse approaches have been used to deduce air-sea and air-land CO_2 fluxes from spatial and temporal gradients in atmospheric CO_2 measurements after accounting for related changes due to transport by using an atmospheric model. Until recently, these inverse approaches have treated fluxes as if they acted uniformly over large areas (Bousquet et al., 2000; Peylin et al., 2005; Patra et al., 2005; Baker et al., 2006). These inverse approaches have yielded estimates of large variability in air-sea CO_2 fluxes over extratropical regions such as the North Atlantic Ocean. Similarly large variability was also found for the same basin by an independent approach, which assumed that fluxes derived from ocean measurements from one time series station in the subtropical gyre, the Bermuda Atlantic Time-Series Station (BATS), were representative of those throughout the basin (Gruber et al., 2002).

Conversely, much smaller variability is simulated by ocean models, which have higher spatial resolution and solve for internal ocean structures while accounting for fundamental processes from first principles. This small basin-wide variability in the North Atlantic air-sea CO_2 flux has been interpreted as being due to compensating patterns within that basin (Le Quéré et al., 2000, 2003a; McKinley et al., 2004b). This interpretation now appears corroborated by a new state-of-the-art atmospheric inversion approach that resolves air-sea CO_2 fluxes on a much finer horizontal grid and also predicts similarly low basin-wide variability (Rodenbeck et al., 2003; McKinley et al., 2004a). With the the older atmospheric inverse approaches, which used very large regions, it now appears more tenuous to use data collected at the

Published by Copernicus GmbH on behalf of the European Geosciences Union.

sparsely spaced atmospheric CO_2 measurement stations to distinguish air-sea versus air-land fluxes. And because variability in air-land fluxes is much larger, any erroneous assignment of that to the ocean causes the variability of air-sea fluxes to be overestimated. However, for inverse approaches with much higher resolution, that error is attributed only to near-coastal regions, which have much smaller surface area. Thus the erroneous net air-sea mass flux is much smaller as well. Therefore both the state-of-the-art atmospheric inversion and the ocean models suggest low variability due to compensating patterns, meaning also that the BATS time series station is inadequate by itself to resolve the integrated basin-wide variability.

Changes in the air-sea CO_2 flux are controlled by atmosphere and ocean dynamics as well as by certain ocean biological processes (photosynthesis, export production, and respiration). Changes in climate are expected to be a primary control of changes in air-sea CO_2 fluxes. Interannual-to-decadal changes in climate over the North Atlantic basin are dominated by the North Atlantic Oscillation (NAO) (Hurrell et al., 2003a). The ocean responds to the NAO with a resulting frequency-dependent signature (Visbeck et al., 2003). The ocean may even have a small feedback on NAO through internal changes and changes in sea ice (Czaja et al., 2003; Deser et al., 2000; Lu and Greatbatch, 2002). This complex climate system affects the marine ecosystem, e.g., through changes in circulation and mixed layer depth (Joyce et al., 2000; Marsh, 2000; Le Quéré et al., 2003b). These processes affect nutrient and light availability and thus export production (Dutkiewicz et al., 2001; Oschlies, 2001). Thus, air-sea CO_2 flux rates should depend on the NAO, which drives changes in temperature, wind stress and wind speed, and ice cover.

Despite these logical climate connections though, McKinley et al. (2004b) found little correlation between NAO and their simulated air-sea CO_2 flux, whose first EOF explained only 11% of the interannual variance. They state that this poor correlation is largely due to the slow air-sea CO_2 exchange equilibration time that acts to decouple the air-sea flux from the climate forcing. Yet if we could account for this and other possible delays, there might be a higher correlation than indicated by EOF analysis, which by definition neglects time lags of the response to the forcing.

Here our aim is to further explore the spatiotemporal structure of interannual variability in the air-sea CO_2 flux within the major regions of the North Atlantic, as simulated by two new 55-year ocean carbon cycle simulations. To do so, we take advantage of an analysis tool that is capable of accounting for temporal lags in the systen and extracting different modes of variability. Lags are induced not only by the slow air-sea exchange time for CO_2 but also by lateral and vertical transport within the ocean (Palter et al., 2005). Such lags should be considered when analysing the causes of variability of air-sea CO_2 fluxes. Secondly, we offer a first attempt to describe decadal oscillations of the air-sea CO_2 flux by exploiting longer 55-year simulations; conversely, decadal variability cannot be extracted from previous 20-year simulations or the comparable length data record from BATS.

2 Methods

2.1 Models

We used the global-ocean general circulation model known as ORCA2, a generic acronym for OPA (Océan Parallélisé), namely version 8.2 (Madec et al., 1998). The ORCA2 model is coupled to the dynamic-thermodynamic Louvain-la-Neuve Ice Model (LIM) (Timmermann et al., 2005). ORCA2 has a nominal 2° horizontal grid resolution in the extratropics, with meridional resolution increasing to 0.5° at the equator. In the Southern Hemisphere away from the equator, ORCA2 employs a $2° \times 2° \cos\theta$ horizontal rectangular grid. In the Northern Hemisphere, the horizontal grid is similar but contorted to have two northern grid singularities over land (one over Asia and another over North America). That geometry maximises the grid spacing and thus the time step around the otherwise troublesome North Pole and thus avoids the conventional filtering that induces numerical problems in the same area. ORCA2 also has 30 vertical levels, 20 of which are in the upper 500 m. The equation of state is calculated using the algorithm of Jackett and McDougall (1995). The bottom boundary layer parameterisation of Beckman and Doscher (1997) was used to represent the flow of deep water over bathymetry. This is the same model configuration as used in previous study of interannual variability (Rodgers et al., 2004) except that here the model also includes a free surface formulated to conserve salt globally (Roullet and Madec, 2000). Lateral mixing is oriented along isopycnal surfaces and includes the mesoscale eddy parameterisation of Gent and McWilliams (1990), except where that is relaxed between 10° S and 10° N. Vertical mixing relies on the turbulent kinetic energy (TKE) scheme of Blanke and Delecluse (1993). Modelled surface salinities are restored to climatological values (Boyer et al., 1998). However with only that restoring, the global integral of the restored surface freshwater flux would not necessarily conserve global ocean volume. Hence we computed the globally averaged change in sea level height at the end of each year. Then during the following year, we applied a corrective (negative) flux (uniform in space and time) over the surface ocean. Thus the model conserves ocean volume over our multi-decadal integrations.

Blanke et al. (2005) evaluated the ability of the ORCA2 model to simulate properties of subtropical mode waters in the North Atlantic, finding reasonable agreement with available observations. Timmermann et al. (2005) focused on the higher latitudes using a similar ORCA2 model configuration and forcing. Generally the ORCA2 model appears to properly simulate seasonal and interannual changes in ice growth and decay, particularly in the Northern Hemisphere. Sites

of deep convection also appear realistic. On the other hand, the width of the Arctic Ocean Boundary Current is overestimated, as is that for the Antarctic Circumpolar Current. The ORCA2 model reproduces both the amplitude and timing El-Niño variability (Lengaigne et al., 2002). However, as with previous ocean modelling studies of interannual variability, our results may be adversely affected by the coarse model resolution and deficiencies in the forcing fields themselves. Much higher horizontal resolution would be needed to properly simulate the position and recirculation patterns of the Gulf Stream (Griffies et al., 2001; Maltrud and McClean, 2005).

The ocean circulation model is coupled online to the biogeochemical-ecosystem model known as the Pelagic Interaction Scheme for Carbon and Ecosystem Studies (PISCES), which has twenty-four compartments (Bopp et al., 2003, 2005; Aumont and Bopp, 2006). Five of these compartments are nutrients that limit phytoplankton growth: nitrate plus ammonium, phosphate, silicate, and iron. Yet phosphate and nitrate+ammonium are not independent. They are linked by constant Redfield ratios. However, the nitrogen pool is also affected by nitrogen fixation and denitrification. Setting these two processes to zero would mean that the distribution of nitrogen and phosphate would differ only by the constant Redfield ratio, given equivalent global sizes for these two pools. PISCES also includes four living compartments. These functional groups include two phytoplankton size classes (nanophytoplankton and diatoms) and two zooplankton size classes (microzooplankton and mesozooplankton). For phytoplankton, prognostic variables include total biomass, iron, chlorophyll, and silicon contents. Thus the model predicts the Fe:C, Chl:C, and Si:C ratios of both phytoplankton groups. For zooplankton, only the total biomass is modelled explicitly. For all species, their internal O_2:C:N:P ratios are assumed to be constant and not to vary. The bacterial pool is not included.

Additionally, PISCES includes three non-living compartments: small sinking particles, big sinking particles, and semi-labile dissolved organic matter. As with the living compartments, constant C:N:P ratios are imposed and are not modelled explicitly. Conversely, the iron, silicon, and calcite pools of the particles are modelled explicitly and their ratios are allowed to vary. Calcite and biogenic silica are assumed to have the same sinking speed as do big particles. In PISCES, all the non-living compartments aggregate as a function of turbulence and differential settling.

In addition to these ecosystem variables, PISCES also carries tracers for dissolved inorganic carbon (DIC), total alkalinity, and dissolved O_2. A complete description of the PISCES model is provided by Aumont and Bopp (2006).

2.2 Simulations

To model interannual variability, we forced our simulations with interannually varying reanalysis fields from the National Centers of Environmental Prediction (NCEP) during 1948–2002 (55 years). The PISCES model was first integrated offline for 5000 years using climatological circulation fields (from ORCA2) while atmospheric CO_2 was held at 278 ppmv. At the end of this period, the model tracer fields had reached a near-steady state, which we arbitrarily defined as being the preindustrial state (year 1838). From 1838, it requires three consecutive 55-year cycles to reach the final year of our simulation, 2002. Thus for this industrial era (1838 onward), a "historical" simulation was made where the model's atmosphere was forced to follow observed annual mean CO_2, as provided by the OCMIP-3/NOCES project. Secondly, we made a "control" simulation where atmospheric CO_2 was maintained at 278 ppmv. From the start of 1838 until the end of 1947 (the first two 55-year cycles), we used climatological circulation fields, offline. We present results from both simulations from the third 55-year cycle (1948 to 2002) where PISCES was integrated in the online model. The daily-mean wind-stress fields for the NCEP reanalysis (Kalnay et al., 1996) are used to force the ocean model at the surface. The wind speeds used for heat and evaporative fluxes in the bulk formulas as well as for gas exchange are calculated from the daily NCEP zonal and meridional components of the 10-m winds.

2.3 Analysis

To analyse complex spatiotemporal structures and potential correlations between fields, we used Multi-channel Singular Spectrum Analysis (MSSA, Plaut and Vautard, 1994). Previously MSSA has been used to extract time dependent structures of climate variables over the North Atlantic (Moron et al., 1998; Avoird, 2002; Da Costa and de Verdière, 2002). MSSA naturally accounts for lags, intermittency of oscillations, and frequency dependencies such as those that characterise ocean and atmospheric variability of the North Atlantic. A detailed description of MSSA is provided in the Appendix.

Here we have used MSSA to extract the natural modes of variability that have signatures in space and time. We decomposed the full signal into oscillations, nonlinear trends, and white noise. Each oscillation represents a possible mode of variability having a specific period, space-time signature, and intermittency. MSSA goes beyond the classical decomposition with Empirical Orthogonal Functions (EOF) because it is able to extract anomalies that propagate in time as well as in space. Another advantage of MSSA is that it imposes no a priori assumption of spatiotemporal structure, as opposed to a less sophisticated spatiotemporal analysis tool known as Principal Oscillation Pattern (POP) (Hasselmann, 1988) that imposes certain temporal oscillations.

To analyse interannual-to-decadal variability of the air-sea CO_2 flux we treated all variables of interest simultaneously, using monthly averages. Thus we avoid using a simple NAO

index that may not be representative of the NAO (Jones et al., 2003), much less total variability over the North Atlantic. In climate studies, it has been shown that the two dominant driving variables in terms of what causes variability at the air-sea interface are the sea surface temperature (SST) and sea level pressure (SLP) (Czaja et al., 2003). The SLP affects both wind stress and wind speed, terms that are used in the model's formulations for exchange of momentum and gases across the air-sea interface. Thus we used SST, wind stress modulus, and the CO_2 flux at the three primary variables in our MSSA analysis.

Prior to making the MSSA analysis, model output was first preprocessed by taking 6-month unweighted running means, then removing the annual cycle and the overall linear trend. Then as a second step in preprocessing, we used EOF analysis (also called Principal Component Analysis) to reduce the number of degrees of freedom from the total number of ocean surface grid points to only 15. This sample size reduction is a practical necessity to reduce computational cost, yet it maintains the key information on variability that is needed for MSSA analysis. As a final step before applying the MSSA analysis, we normalised all variables independently simply because they have different units. For the dominant climate variables (SST and wind stress), known as the active variables, the normalised amplitudes were assigned a weight of 1; for all other variables, denoted as passive variables, normalised amplitudes were assigned weights of 0.1. Furthermore, because the MSSA analysis is based on variances of amplitudes, the effective weight for passive variables is actually one hundred times lower than for active variables. This arbitrary weighting scheme ensures that passive variables will have negligible influence on active variables, without being considered as numerically insignificant. In other words, this weighting scheme ensures that despite simultaneous analysis of all variables, MSSA treats passive variables as being driven by the active variables. For instance, the air-sea CO_2 flux is driven by climate variability and not the contrary. This weighting scheme preserves the same structure for the dominant modes of any active variable throughout our analyses. For example, we will show that after MSSA analysis, the SST anomalies from both simulations have the same amplitudes even though variability of air-sea CO_2 flux is different. Our sensitivity test using a weight of 0.5 instead of 0.1 for the passive variables did not qualitatively change the conclusions that result from this analysis..

Within the MSSA itself, the essential parameter is the width of the temporal window M (see Appendix). Typically one uses a width of 0.1 to 0.5 times the length of analysis period. Wider windows resolve oscillations with longer periods. The best choice of M was found by using different values and evaluating the stability of results. After testing values ranging from 72 to 156 months, we settled on a window width of 96 months, which was able to resolve simultaneously both interannual modes and the decadal mode that were apparent when using different values of M.

Once the MSSA analysis is complete, one is left with statistical modes that can be grouped or studied separately. Oscillations are identified as pairs of modes having similar characteristics. MSSA assumes that the variability is not highly nonlinear. We demonstrate in Sects. 3.6 and 3.7 that nonlinearities here are typically small. Thus our linear decomposition appears appropriate.. In subsequent sections, we discuss results from the MSSA analysis applied to the historical simulation. In some cases we also compare that analysis to analogous results from the control simulation.

3 Results

3.1 Annual cycle

As a prerequisite to simulating interannual variability, a model should first be able to simulate a reasonable annual cycle. Figure 1 compares results from our historical simulation to data-based monthly maps of ΔpCO_2 (Takahashi et al., 2002) in the North Atlantic. Generally, the trends seen in the model are similar to those observed. In winter, the whole basin acts as a sink for the atmospheric CO_2. The lowest values are found at the southern and northwestern boundaries. In summer, the southern part of the basin becomes a source. Yet this comparison also reveals deficiencies particularly where the Gulf-Stream is observed to be most intense, southeast of Newfoundland. As with other coarse-resolution models, the Gulf Stream is too weak and continues flowing northward when it should break off to the east. These dynamical problems contribute to model-data differences in terms of the air-sea flux. During winter, the simulated air-to-sea flux is too large in the west; during summer it is redistributed along the American coast, thereby affecting the amplitude of the annual cycle.

3.2 Variability at the BATS station

When interannual anomalies of the air-sea CO_2 flux are integrated globally, the range of the variability is $\pm 0.5\,\mathrm{Pg\,C\,yr^{-1}}$ and the standard deviation σ is $0.25\,\mathrm{Pg\,C\,yr^{-1}}$. These results are consistent with global variability estimates from other models (McKinley et al., 2004b; Wetzel et al., 2005). For the North Atlantic, the basin-wide variability in ORCA2 (σ=0.045 $\mathrm{Pg\,C\,yr^{-1}}$) is 50% higher than that found by McKinley et al. (2004b).

The only time series station available to evaluate interannual variability in the North Atlantic is at BATS. Figure 2a reveals that the amplitude of modelled variability is much less than that observed, except during the late 1990's. On the other hand, the simulated phasing appears more realistic. Other models appear to show a somewhat higher amplitude, but similar phasing.

To go beyond these qualitative statements, we quantified agreement with a Taylor diagram (Taylor, 2001) for BATS, which compares overall summary statistics between models

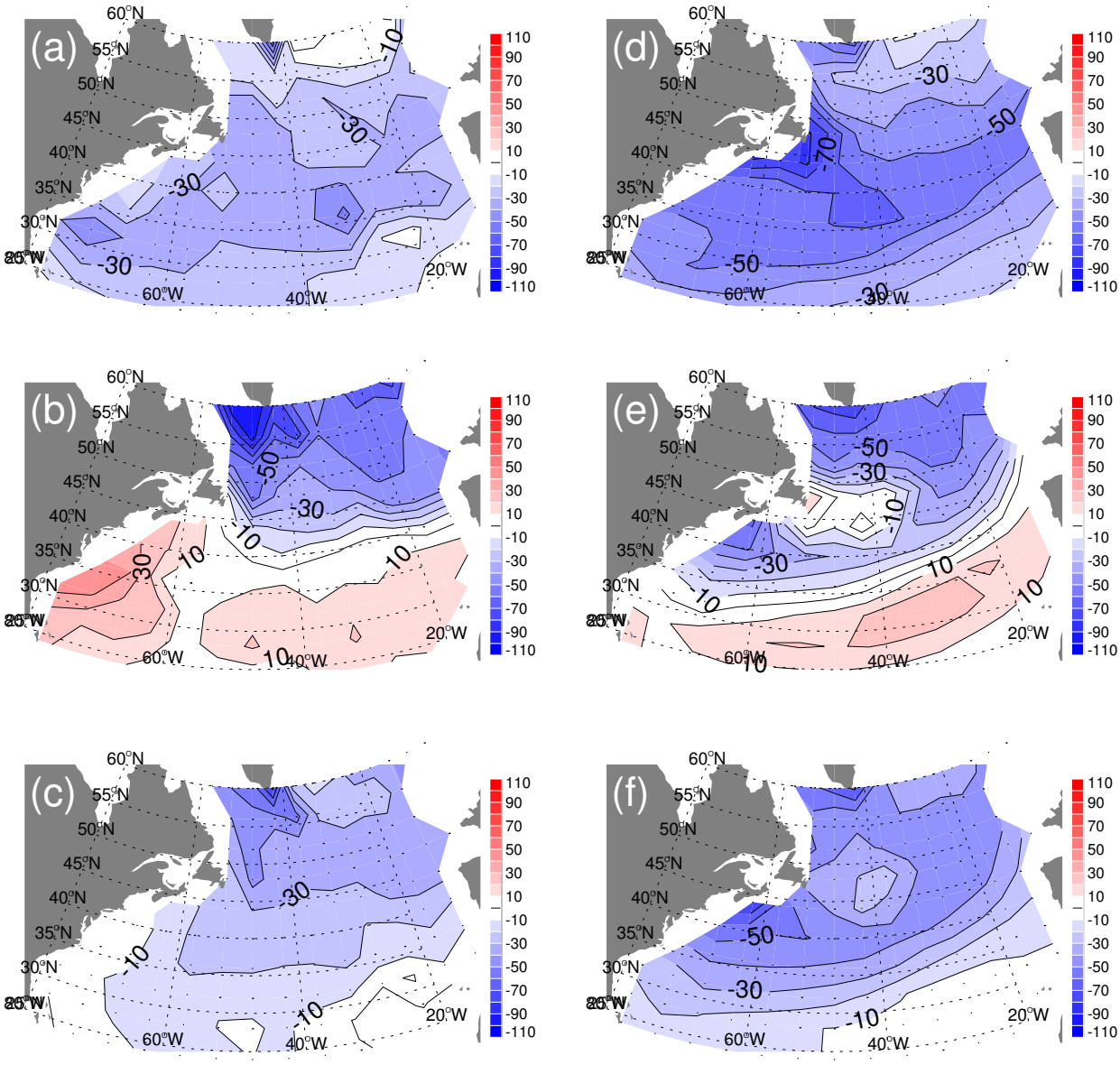

Fig. 1. Climatological maps of ΔpCO_2 in µatm for **(a)** winter, **(b)** summer, and **(c)** the annual mean from observations (Takahashi et al., 2002) versus the simulated averages for **(d)** winter, **(e)** summer, and **(f)** annual mean over the last 55-year cycle. Results are mapped using the Lambert equal-area projection.

and data (Fig. 2b). That analysis reveals that all models systematically underestimate the observed variability and that there are large differences between models. The MIT model exhibits about 2/3 of the overall observed variability whereas the other models reach less than 1/3, with ORCA2 being the lowest. Interestingly that trend is reversed when variability is integrated over the entire North Atlantic (north of 15° N): for MIT, the standard deviation σ=0.03 PgC yr^{-1} (McKinley et al., 2004b) whereas for ORCA2 σ=0.045 Pg C yr^{-1}). Thus the variability at BATS does not appear to be a good quantitative indicator of the basin-wide variability in the North Atlantic. Of course, the amplitude is only part of the story and phasing also matters. Most correlated with the observed phasing at BATS is the ORCA2 model (r=0.52), whereas phasing is less realistic for MIT (r=0.30).

As a further test to see if these trends in model-data differences are representative of subtropical gyres in general, we made a similar analysis for the ALOHA station in the Pacific (Fig. 3). Both the amplitude and the phasing of simulated variability at ALOHA is generally more like that observed. To demonstrate to what extent the amplitude of BATS variability is representative of that across the North Atlantic,

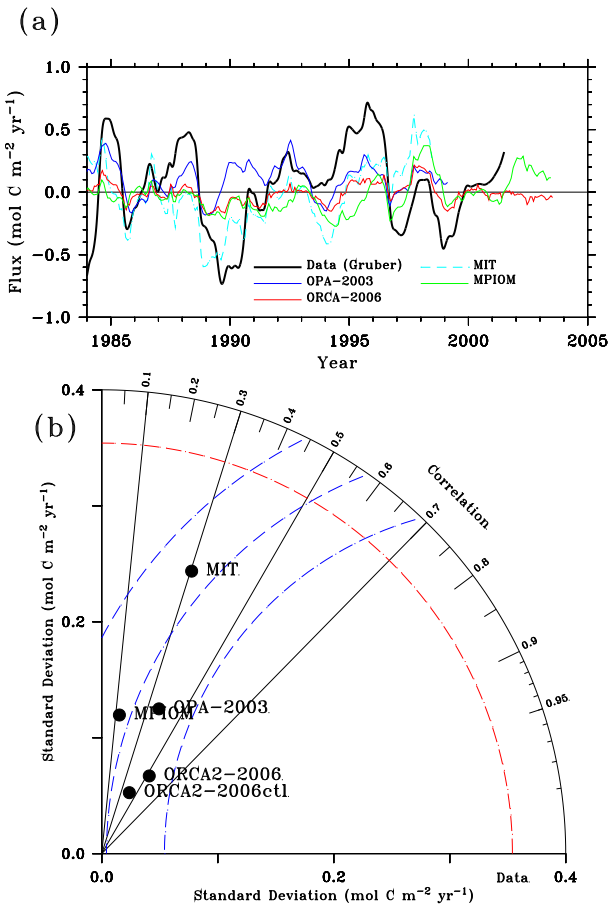

Fig. 2. **(a)** Times series of the anomaly of the sea-to-air CO_2 flux [mol C m^{-2} year^{-1}] at BATS (32° N, 64° W) for the observations (Gruber et al., 2002), our historical simulation (ORCA-2006) as a 2°-box average around BATS as well as results from the three previously published ocean model simulations: OPA-2003 (Le Quéré et al., 2003b), MPIOM (Wetzel et al., 2005) and MIT (McKinley et al., 2004b). Anomalies are derived by computing a 12-month running mean then removing the climatological annual cycle. **(b)** Taylor (2001) diagram comparing models to data at BATS. In this polar plot, the radial axis represents the standard deviation, a measure of the overall amplitude (where the data reference is the red-dashed curve); the angular axis is the correlation r to the observations (where for perfect phasing r=1.0); and the distance between the data reference (where the red-dashed curve intersects the bottom axis) and any model point (see blue dashed curves) is the central pattern RMS error, a common measure of overall model-data agreement (RMS isolines are given as blue dashed curves).

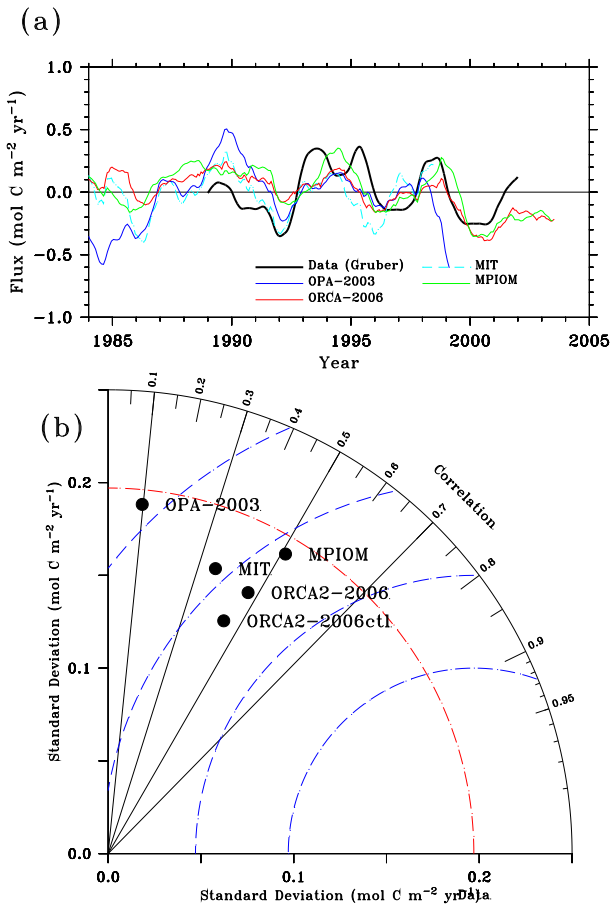

Fig. 3. Same as Fig. 2 but for ALOHA station [19° N , 158° W] (with observations from Brix et al., 2004).

Fig. 4 shows a map of the standard deviation of the simulated monthly anomalies (relative to the climatological monthly mean) of the air-sea CO_2 flux. Standard deviations are much lower than average in the subtropics, where BATS is located.

3.3 Relationship between the NAO and the air-sea CO_2 flux

In the North Atlantic, McKinley et al. (2004b) found little correlation between the NAO and the air-sea CO_2 flux, with the first EOF explaining only 11% of the total variance. However, there could be a larger correlation than revealed by EOF analysis, which neglects lags in the response of air-sea CO_2 flux to the NAO climate forcing. To explore this possibility, we first computed lag correlations between the NAO and the area-integrated air-sea CO_2 flux in the subtropical gyre as well as in the intergyre region (Fig. 5). In the subtropical gyre, the largest correlation was indeed found at zero lag (r=−0.56±0.05, 95% confidence interval). However, in the intergyre region, the maximum correlation is found with a lag of 2.5 years (r=0.43±0.06). In the subpolar gyre, the correlation is r=−0.31±0.07 near zero lag. Furthermore, the spatial inhomogeneity of these lags may result in compensations between regions at zero lag. Thus basin-wide extrapolation from BATS results is unable to provide a reliable estimate of the total basin-wide variability of the air-sea CO_2 flux in the North Atlantic. It will be shown in Sect. 3.5 that simulated CO_2 fluxes lag the climate forcing by up to 3 years.

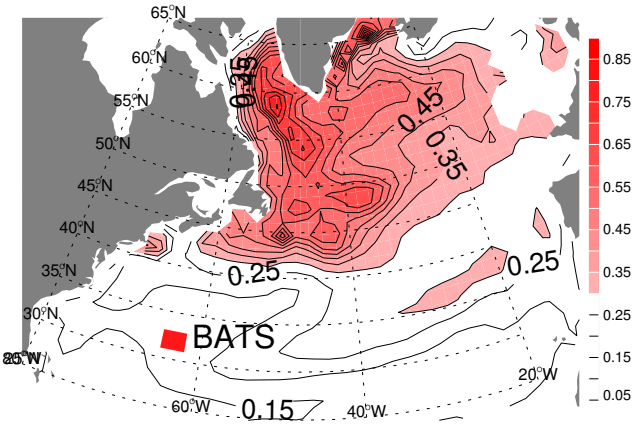

Fig. 4. Map of the standard deviation of the monthly anomalies of the air-sea CO_2 flux [mol C m^{-2} year^{-1}] simulated in the historical simulation. A solid square indicates the position of the BATS station.

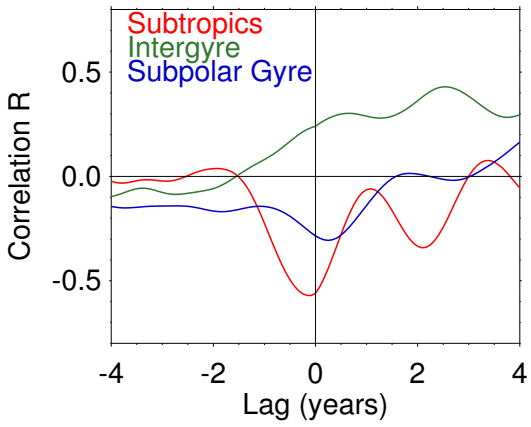

Fig. 5. Lag correlation between the NAO index and the air-sea CO_2 flux in the subtropical region, bounded by 65° W–43° W and 29° N–37° N (red) as well as the intergyre region, bounded by 54° W–21° W and 45° N–52° N (green), and the subpolar region bounded by (65° W–43° W, 55° N–60° N) (blue). White noise was removed by MSSA prior to this lag correlation analysis (see Sect. 2.3).

Figure 6 shows that despite the subpolar gyre's smaller areal extent, the standard deviation of the variability of its area-integrated air-sea CO_2 flux is 20% larger than that for the subtropical gyre (see also Fig. 4). Concerning timing, some major events do occur simultaneously in both gyres, yet such is far from being a general rule (Fig. 6). Additionally, there is more low frequency variability in the subpolar gyre relative to the subtropical gyre. In summary, our simple analysis so far indicates that lags, perhaps due in part to horizontal transport, should be considered and that both gyres differ and should be analysed separately.

To properly describe variability of air-sea CO_2 fluxes in the North Atlantic, we need a method that accounts for correlations between variables having complex spatiotemporal structure. Furthermore, we need to distinguish interannual from decadal variability.

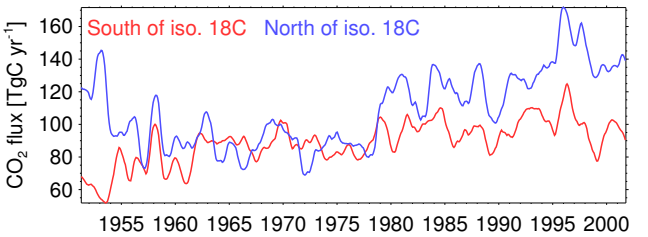

Fig. 6. Times series of the area-integrated CO_2 flux [Tg C year^{-1}] over the subtropical gyre (red) and over the intergyre plus subpolar gyre (blue). For simplicity, the limit between the two regions was arbitrarily defined here as the climatological annual mean 18°C surface isotherm. Shown are 12-month running means in order to remove high frequency variability.

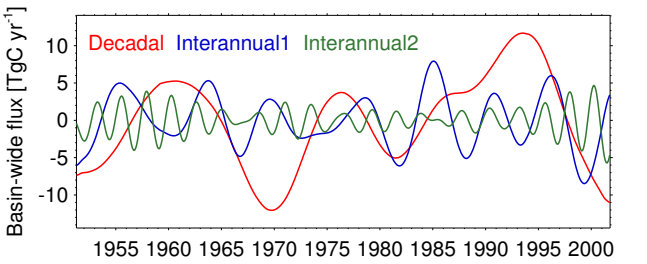

Fig. 7. Anomalies of the basin-wide integrated CO_2 flux (between 20°N and 70°N) in Tg C year^{-1} for the ∼3.2-year interannual model (green), the 5–7 year interannual mode (blue), and the 13-year decadal mode (red).

3.4 Spectral properties

We evaluated the total contribution of each of the dominant oscillations extracted by MSSA in terms of the area-integrated, air-sea CO_2 flux (Fig. 7). The signal is decomposed into four major modes: (1) a first "interannual" oscillatory mode with a 3.2-year period representing 5.0% of the total variance; (2) a second "interannual" oscillatory mode with a 5–7 year period representing 6.4% of the total variance; (3) a "decadal" mode with a period of around 13 years which contributes 12.7% to the total variance and is the dominant oscillatory mode; and (4) an "interdecadal" mode (not shown) represented by a single non-oscillatory MSSA mode (a nonlinear trend) that contributes 14% to the total variance of air-sea CO_2 flux. The latter includes effects due to slowly varying climate forcing, and has already been identified in observational analyses (Moron et al., 1998). Although the decadal mode is not as well resolved as the interannual modes, as expected given just a 55-year time series, its spatiotemporal characteristics persist despite changes in the MSSA window parameter. Hence the decadal mode is

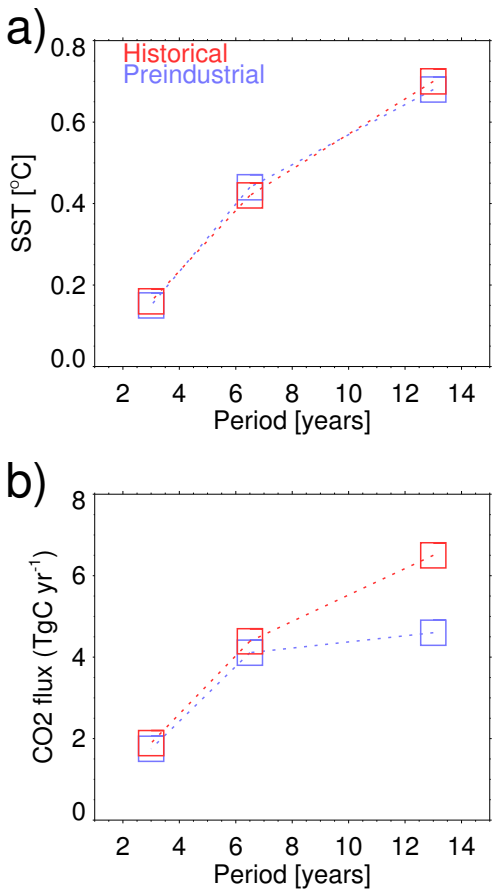

Fig. 8. The amplitude of anomalies for **(a)** maximal SST (°C) and **(b)** basin-wide integrated air-sea CO_2 flux , between 20° N and 70° N (Tg C year^{-1}) for the control and historical simulations, plotted against the period for each mode.

statistically significant. Furthermore, the frequencies of the MSSA-derived decadal mode and the two interannual modes are typical for NAO spectra (Hurrell et al., 2003b). Both the decadal mode and 5–7 year interannual mode were reported by Moron et al. (1998). Additionally, variability at ∼3-year and ∼7-year frequencies was already found for the response of ocean heat transport to the NCEP reanalysis forcing (Gulev et al., 2003).

Figure 8 shows the amplitude of anomalies for SST where its values are maximal and the basin-wide integrated air-sea CO_2 flux, plotted against the average period of each mode. Both simulations yield essentially identical results for all climate variables, including SST and wind. Such would not necessarily occur given that MSSA analyses all variables simultaneously and each affects the others, including the air-sea flux of CO_2 which differs between the two simulations. The absence of substantial differences demonstrates the effectiveness of our weighting scheme, namely a weight of 0.1 for the air-sea flux of CO_2 (see Sect. 2.3).

For the air-sea CO_2 flux, differences between simulations are also negligible for the two interannual modes. In contrast, the amplitude of the basin-wide integrated air-sea flux of CO_2 decadal variability is 30% larger in the historical simulation relative to the control. Thus decadal variability of air-sea CO_2 fluxes in the North Atlantic has followed the increase in atmospheric CO_2 and could continue to increase its dominance over interannual variability with further CO_2 increases in the future. Similarly, this change in decadal variability can be explained in terms of the anthropogenic change in ΔpCO_2 (see Sect. 3.7).

3.5 Spatiotemporal description

Here we consider the inherent properties of the 3 oscillatory modes (2 interannual modes and the decadal mode) of variability, each of which is an oscillation that is a repeated cycle over the length of the simulation. To provide greater physical meaning to our analysis and improve statistical significance, we chose not to interpret the spatiotemporal structure of the modes at a given time during the simulation. Instead, we made composites cycles, i.e., an averaged cycle for each mode (see Da Costa and Vautard, 1997). Each composite cycle was decomposed into 8 parts (phases) in order to evaluate its spatiotemporal evolution. For example, such an approach is commonly used to compute an annual cycle with 12 phases (monthly) decomposition. Our composites for the decadal mode are shown in Fig. 9 whereas those for the two interannual modes are shown in Figs. 10 and 11.

We provide composite maps only for SST and the air-sea CO_2 flux. Maps of wind stress modulus anomalies are not shown because they add little new, relevant information. We chose to display composite maps at only 2 of the 8 phases (a transitory phase and an extreme phase) because one does not loose information by summarising a sinusoidal cycle over a quarter of its period. We arbitrarily define the extreme phase as that when SST anomalies are highest. That always occurs in the 7th part of the 8-phase cycle. We further define the transitory phase as the advance phase quadrature compared to the extreme phase, i.e., the 5th part of the 8-phase cycle.

All modes for SST show features that are characteristic of the NAO (see Hurrell et al., 2003a, and references therein). Wind stress shows the same features but is not displayed. The dominant pattern for SST anomalies is a north-south dipole, particularly in the extreme phase. This dipole results from variability in the Gulf Stream position. This pattern is associated with a variability of the strong westward winds (not shown) over the subpolar gyre. These winds are closely related to the variations in the NAO index. Although there are differences in this dipole among the three dominant modes, differences concern mainly the transitory phases and do not affect their NAO-like signature. Our 5–7 year interannual mode shown in Fig. 10b is similar in structure to the 7.7-year mode of Da Costa and de Verdière (2002).

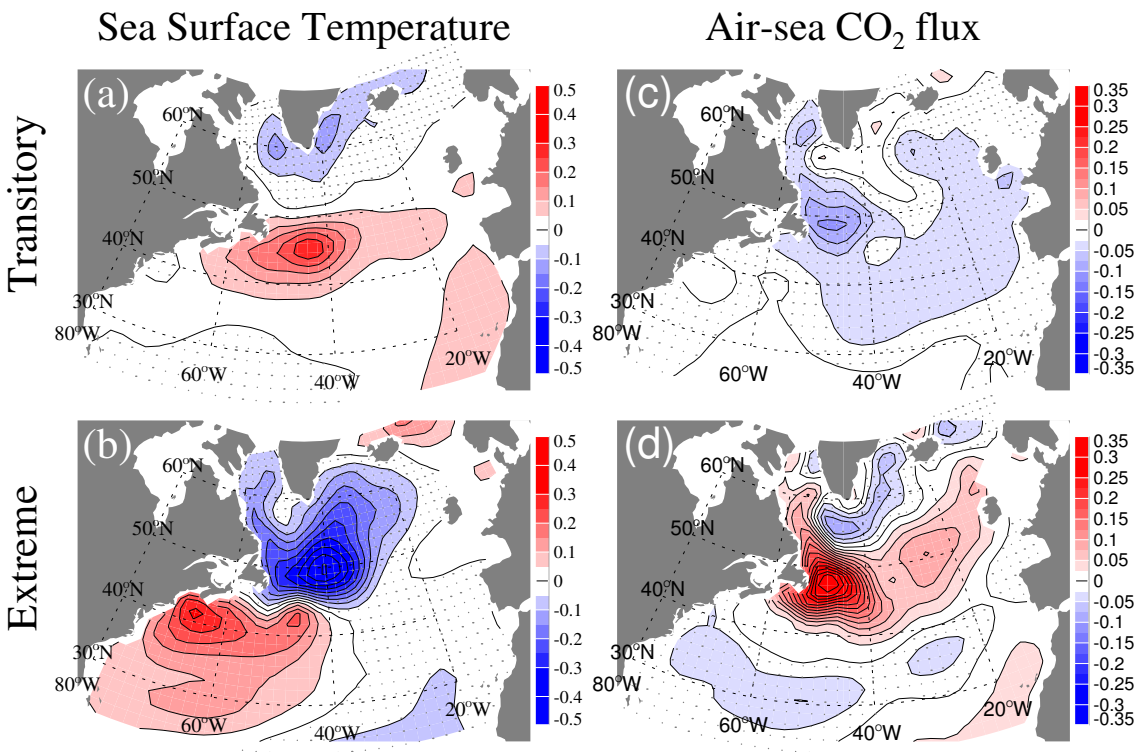

Fig. 9. Anomalies of SST [°C] for the decadal mode during the **(a)** transitory and **(b)** extreme phases of the 8-phase cycles. Corresponding maps are also shown for the **(c)** transitory and **(d)** extreme phases for anomalies of the air-sea CO_2 flux [mol C m^{-2} $year^{-1}$]. Negative values are indicated by dotted areas. A transitory phase occurs a quarter of a cycle before an extreme phase.

South of 35° N, air-sea CO_2 flux anomalies generally follow SST anomalies in all modes and phases. Such SST dependence is known for the annual cycle in the subtropical gyre (Takahashi et al., 2002). In this latitude range, CO_2 flux anomalies have similar amplitudes at all frequencies. Anomalies having different signs often partly cancel one another between the east and the west (e.g., see Fig. 9d).

North of 35° N, there exists no clear relationship between anomalies of SST and those of the air-sea CO_2 flux. Thus outside of the subtropical gyre, the system is more complex in terms of what drives interannual-to-decadal variability of air-sea CO_2 fluxes. Northern anomalies for the air-sea CO_2 flux are much larger for the decadal mode than for the interannual modes, especially during the extreme phases. The decadal mode is nearly stationary, with large positive anomalies covering the intergyre region and the eastern subpolar gyre; small anomalies of opposite sign are found near Greenland. North of 40° N, the extreme phases of the two interannual modes have some similarities. They exhibit anomalies of one sign in the central intergyre and near Greenland, with anomalies of opposite sign in the eastern and western subpolar gyre (Figs. 10d and 11d). These anomalies tend to cancel each another. Conversely, for the 5–7 year interannual mode during the transitory phase, anomalies are more homogeneous (Fig. 10). Anomalies in the western portion of the subpolar gyre are larger than those in the eastern subpolar gyre and they have the same sign as eastern subtropical anomalies; these patterns are in sharp contrast with those in the transitory phase of the 3.2-year interannual mode. Thus the 5–7 year interannual mode has air-sea CO_2 flux anomalies, when integrated across the basin, that are larger during the transitory phase than during the extreme phase. This variability is not in phase with the SST and wind stress anomalies.

Complex spatiotemporal patterns mean that anomalies in one part of the basin partially cancel those elsewhere. As an illustration, if we were to neglect the differences in the sign of anomalies, the area integrated, basin-wide, air-sea CO_2 flux would be 2 to 3 times larger in terms of interannual-to-decadal variability. Spatiotemporal complexity also implies lags in the response of the air-sea CO_2 fluxes to climate forcing. For example, where wind speed anomalies are largest, off the coast of Ireland, we evaluated the corresponding lag for the air-sea flux (Fig. 12). Summing all three oscillatory modes, the correlation (r=0.64±0.05 with the 95% confidence interval) is largest when flux anomalies lag wind speed by 1 to 3 years. At zero lag, the correlation is not significant. A 1-year lag may be explained by the roughly 1-year equilibration time between atmospheric CO_2 and mixed-layer DIC concentrations (Broecker and Peng, 1974). Longer lags may

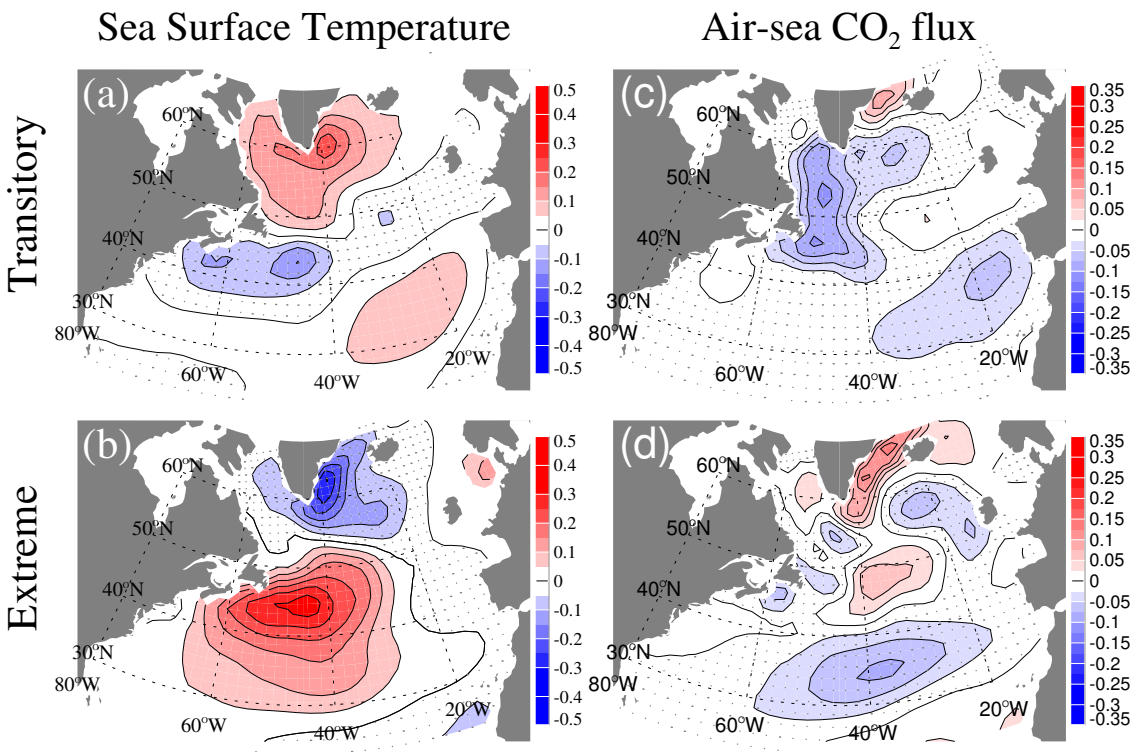

Fig. 10. Anomalies of SST and the air-sea CO_2 flux shown as in Fig. 9, but for the 5–7 year interannual mode.

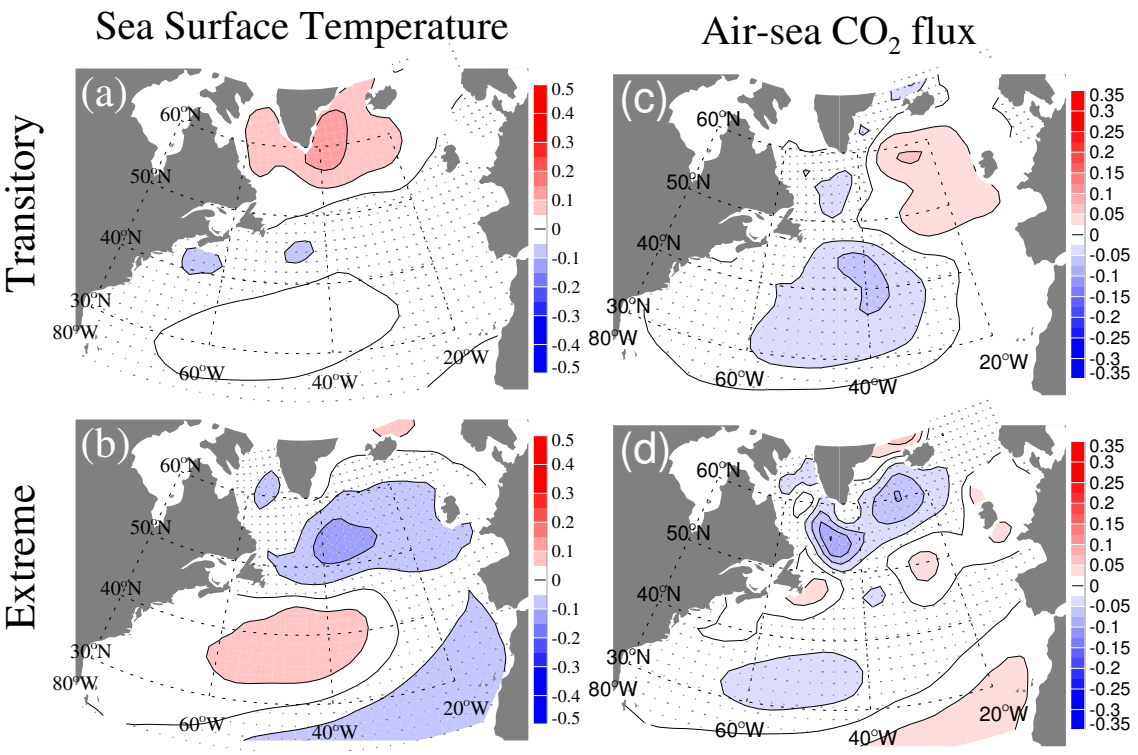

Fig. 11. Anomalies of SST and the air-sea CO_2 flux shown as in Fig. 9, but for the 3.2-year interannual mode.

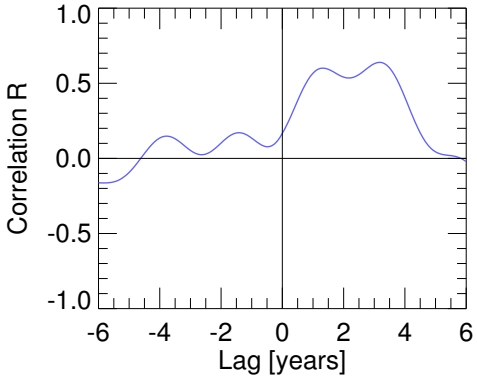

Fig. 12. Lag correlation using the sum of interannual and decadal variability for wind speed off Ireland (where wind anomalies are largest) vs. the air-sea CO_2 flux integrated areally across the basin (20° N to 70° N). Correlation maxima occur when the flux lags wind speed by 1 and 3.1 years.

be due to non-local forcing through horizontal transport of carbon as suggested by Follows and Williams (2004) and as detailed in the Discussion.

3.6 Inferred processes

The large surface area of the subtropical gyre suggests that anomalies there could dominate basin-wide variability of air-sea CO_2 fluxes, if they were not cancelled by anomalies elsewhere. However, we have already showed that intergyre and subpolar air-sea CO_2 flux anomalies are substantial contributors and that those are often opposed to subtropical anomalies. We have also shown that the dominant processes that control anomalies in these regions are probably different.

For insight into what processes control variability of the air-sea CO_2 flux, we decomposed the basic flux equation into means and anomalies. That is, we write the anomaly of the air-to-sea CO_2 flux as

$$F'_{CO_2} = -(Kg \cdot \Delta pCO_2)' = -Kg' \cdot \overline{\Delta pCO_2} - \overline{Kg} \cdot \Delta pCO'_2$$

where Kg is gas exchange coefficient, ΔpCO_2 is the difference between oceanic and atmospheric pCO_2 (partial pressure of CO_2), the prime denotes an anomaly, and the overbar represents the long-term average (over the length of the simulation). The minus signs are necessary because we want anomalies for the air-to-sea flux and not the sea-to-air flux. The anomalies of ΔpCO_2 and Kg were extracted by MSSA. Figure 13 shows zonal integrals of these terms in extreme phases. Additionally, we display these two terms as maps of anomalies for the decadal model, for both transitory and extreme phases (Fig. 14). Because Kg was not an output variable of the model, we computed it from saved monthly means of temperature, salinity, wind speed, and fractional sea ice cover. Weak nonlinearities lead to errors that affect this 2-term linear decomposition of the air-sea flux (with MSSA).

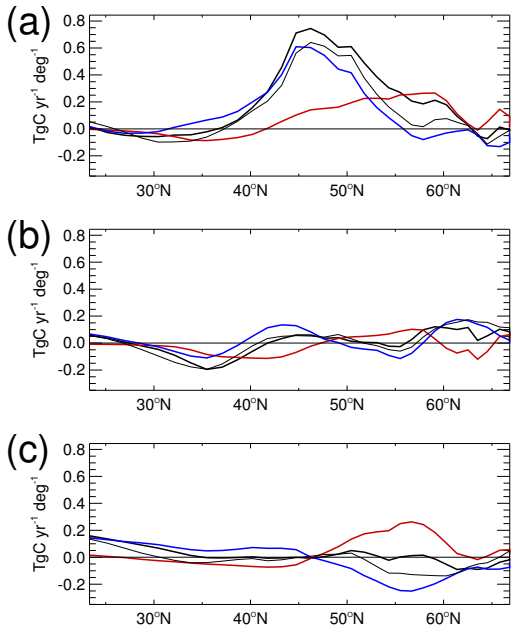

Fig. 13. Zonal integrals in TgC yr^{-1}deg^{-1} for $-Kg' \cdot \overline{\Delta pCO_2}$ (red line), $-\overline{Kg} \cdot \Delta pCO'_2$ (blue line), their sum (thick black line) and the directly estimated air-sea CO_2 flux (thin black line) for the extreme phases of **(a)** the 13-year decadal mode, **(b)** the 5–7 year interannual mode, and **(c)** the 3.2-year interannual mode.

The sum of these two terms is generally similar to the air-sea CO_2 flux estimated directly with MSSA except north of 55° N. The total flux in these northern latitudes is generally small (Fig. 13), and for the decadal mode it is substantially less than that estimated by the the sum of the 2 linear terms. Furthermore, the complex nature of anomalies in this region means that our decomposition and reconstruction may suffer. Yet as shown later, our conclusions from this 2-term linear decomposition are consistent with those from comparison of simulations (Sect. 3.7).

The pattern of the Kg' contribution is similar to that for the wind speed anomaly but it is modulated by SST anomalies. Generally there is a dipolar north-south pattern, with larger values to the north. The contribution due to $\Delta pCO'_2$ is more complex. For the decadal mode, this term dominates during extreme phases with large anomalies having the same sign as those from Kg' over a wide band of latitudes north of 40° N (Figs. 13a and 14d). During transitory phases, the $\Delta pCO'_2$ term is considerably weaker. For the 5–7 year interannual mode, this term is homogeneous over the whole basin during transitory phases (see Fig. 15a), which explains why the area-integrated air-sea CO_2 flux lags the wind forcing (see Sect. 3.5): comparing the map for the $-\overline{Kg} \cdot \Delta pCO'_2$ term to corresponding wind maps reveals that the 5–7 year mode has a 2.5-to-3 year lag between maximal wind forcing (around the extreme phase) and maximal basin-wide integrated flux (around the following transitory phase). This lag is consistent

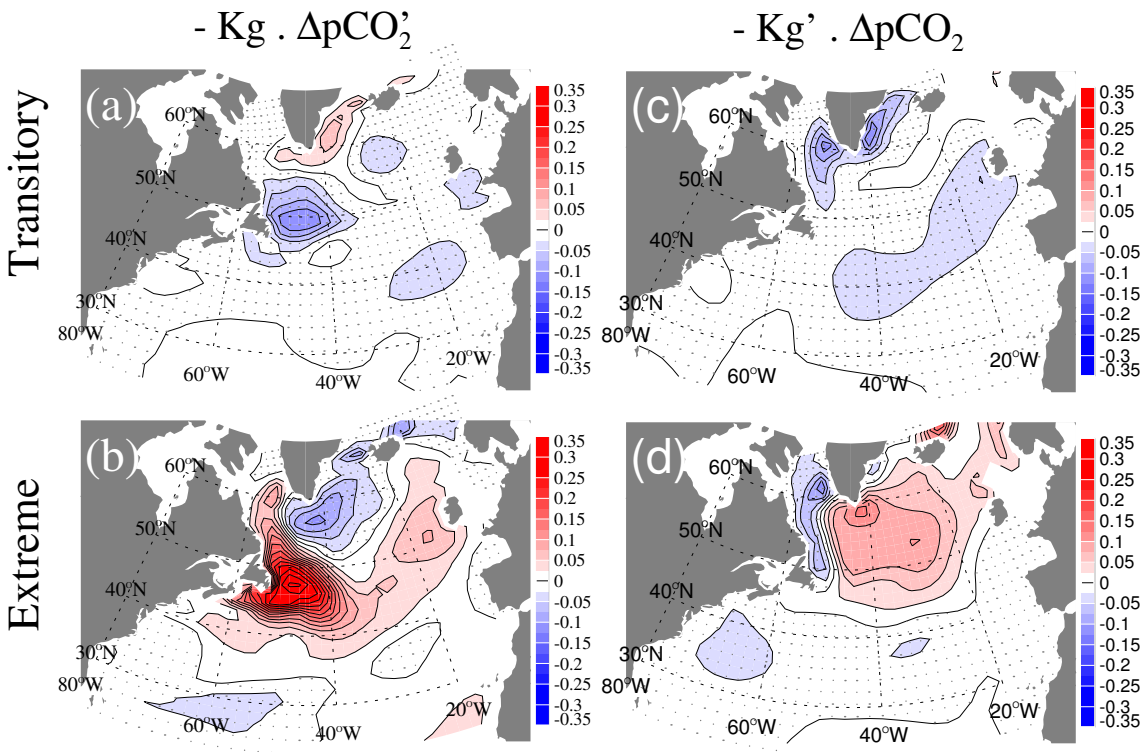

Fig. 14. Decadal mode anomalies for the **(a)** extreme and **(b)** transitory phases of the $-\overline{Kg}\cdot\Delta\mathrm{pCO}_2'$ term as well as the **(c)** extreme and **(d)** transitory phases of the $-Kg'\cdot\overline{\Delta\mathrm{pCO}_2}$ term (in mol C year^{-1} m^{-2}). For each phase, the sum of left- and right-hand maps yields the total air-sea CO_2 flux anomalies shown in Figs. 9c and 9d.

with that shown in Fig. 12. The 3.2-year interannual mode (not shown) is generally weak and the two deconvolved terms tend to cancel one another over the basin.

Another important term is the convective supply of DIC-enriched deep water to the mixed layer. Mixed-layer depth variations may provide a good estimator of such vertical exchange. South of Greenland and throughout much of the subpolar gyre, anomalies of variations in mixed-layer depth for the extreme phase (Fig. 16b) are opposite in sign to those for $-\overline{Kg}\cdot\Delta\mathrm{pCO}_2'$ (Fig. 14b). Therefore, mixed-layer variations appear to be responsible for anomalies of air-sea CO_2 fluxes in this area. Elsewhere, starting from east of Newfoundland to the subtropical gyre, mixing dampens variability of the air-sea CO_2 fluxes.

Deep waters are enriched in nutrients as well as in DIC. Hence variations of the mixed layer depth and greater exchange with deep water also means greater nutrient supply to the surface and thus increased particle export of organic matter. Anomalies of variations in export of large particles reveal that for the extreme phase (Fig. 16d), these variations reinforce the air-sea CO_2 flux over most of the North Atlantic (see Fig. 9d), including the subtropical gyre, the intergyre region, and particularly the western subpolar gyre. In contrast, to the north, around Greenland and Iceland, variations in particle export appear to go against variations in air-sea CO_2 fluxes; however, these trends are compensated by the opposite effect due to variations in mixed layer depth. During the transitory phase of the decadal mode, large homogeneous variations in particle export (Fig. 14c) may explain most of the variability of the air-sea flux (Fig. 9c). This tendency for decadal variability is even more prominent for interannual variability, particularly the longer 5–7 year mode (Fig. 17a). Anomalies in particle export appear to be slightly reinforced by SST anomalies (Fig. 10a), thereby explaining the structure of anomalies of the transitory phase of the $-\overline{Kg}\cdot\Delta\mathrm{pCO}_2'$ term (Fig. 15a). These results suggest a biological link as a likely cause for the delayed response of the air-sea CO_2 flux to the atmospheric forcing. However, these qualitative interpretations must be considered preliminary as others here that are based on matching the sign and structure of mapped anomalies. This qualitative approach provides a first attempt to use MSSA to analyse complex spatiotemporal variability of physical and biogeochemical variables that play a role in controlling air-sea fluxes. Clearly though, there is a need to develop an approach which uses MSSA to quantify the contribution of individual terms to the overall flux.

3.7 Preindustrial versus modern case

As shown in Fig. 8, increased atmospheric CO_2 increases decadal variability of the air-sea CO_2 flux in the North Atlantic. This increased variability results from the effect of the increased absolute value of ΔpCO_2 on the $\overline{\Delta pCO_2} \cdot Kg'$ term. The increase in $\overline{\Delta pCO_2}$ between preindustrial (control simulation) and modern (historical simulation) times, namely the anthropogenic change, is largest north of 30° N (Fig. 18a). Thus relative to the control, decadal variability of the historical run is enhanced in the subpolar region and changes sign in the subtropics and intergyre regions (compare Figs. 18b and 9d). Decadal anomalies have thus become more homogeneous as the area-integrated air-sea CO_2 flux has increased. In brief, differences in the structure of the decadal mode between the low- and high-CO_2 simulations are explained by this decomposition of the air-sea flux equation. That decomposition further reveals that MSSA is able to consistently extract the decadal mode under different conditions. In the future, as atmospheric CO_2 continues to increase, so will the magnitude of $\overline{\Delta pCO_2}$, thereby increasing the contribution of the $-\overline{\Delta pCO_2} \cdot Kg'$ term, particularly at decadal timescales.

4 Discussion

There appear several possible reasons for why ocean models may systematically underestimate variability at BATS (Fig. 2). To start with, although the models are imperfect, there are also uncertainties with the data-based estimates for air-sea CO_2 fluxes at BATS, which are not measured directly. That is, they are derived from other carbon system measurements, a diagnostic model, and a gas transfer coefficient based on wind speed that has substantial uncertainty (Gruber et al., 2002).

Second, horizontal model resolution could be inadequate, especially near the western boundary. All ocean models that have been used to study interannual variability of air-sea CO_2 fluxes have coarse horizontal resolution, meaning they do not explicitly simulate mesoscale eddies. Higher horizontal resolution might well improve model deficiencies concerning the simulated annual cycle in the air-sea CO_2 flux adjacent to North America in the subtropical gyre and intergyre region. Likewise, higher resolution could alter the large simulated decadal anomalies in this region as well as those to the north. In the region south and east of Newfoundland, it has been documented that mesoscale dynamics affect DIC content as well as other biogeochemical properties (McGillicuddy Jr. et al., 1999; Bates, 2001; Mahadevan et al., 2004).

Third, the ocean models may underpredict variability due to inadequacies in the atmospheric reanalysis fields that are used to force them. For instance three of the four models shown in Fig. 2 used wind fields from the NCEP reanalysis (OPA-2003 is the only exception). The only other long reanalysis data product, ERA40 from the European Centre for

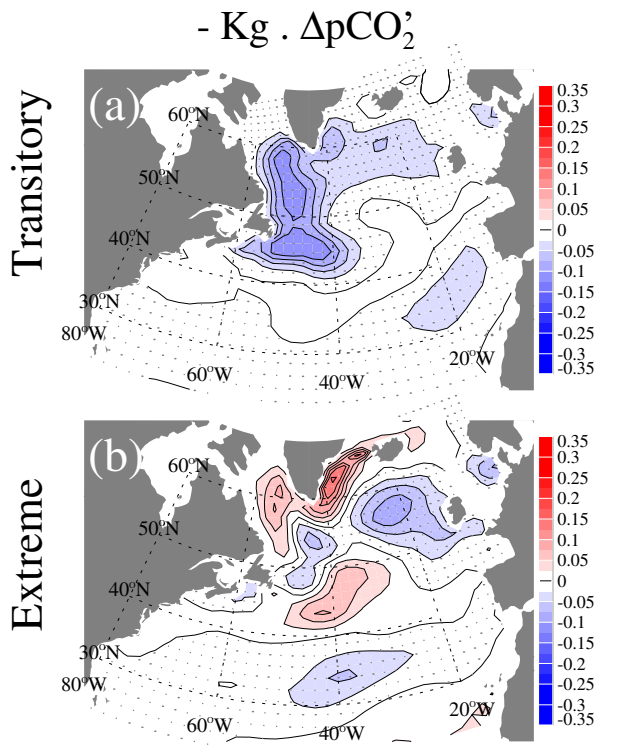

Fig. 15. The 5–7 year interannual mode anomalies for the **(a)** extreme and **(b)** transitory phases of the $-\overline{Kg} \cdot \Delta pCO_2'$ term (in mol C year^{-1} m^{-2}).

Medium-Range Weather Forecasts (ECMWF) became available after our simulations had already been initiated. Comparison over the North Atlantic (Fig. 19) reveals that NCEP underestimates the amplitude of interannual variability of ERA40 wind speeds by more than a factor of three. NCEP wind speeds are also less intense than those measured along ship tracks from the World Ocean Circulation Experiment (WOCE) (Smith et al., 2001). On a wider scale, the subsampled NCEP reanalysis data predicts only half of the observed interannual variability in annual, zonal-mean meridional atmospheric transport computed from observational sites, perhaps caused in part by filtering during the NCEP reanalysis initialization process (Waliser et al., 1999). Damping of variability in the NCEP reanalysis data may also result from other aspects of the data assimilation procedure and the 6-h storage frequency.

Finally, if forcing is indeed a problem, then weaker NCEP forcing northward of 40° N could lead to weaker lateral infiltration of mode waters from higher latitudes and hence less variability at BATS. Variability of forcing at 40° N may well affect tracer concentrations at the base of the mixed layer at BATS (Palter et al., 2005). Weak forcing combined with lateral transport would also affect lags that are inherent in the system.

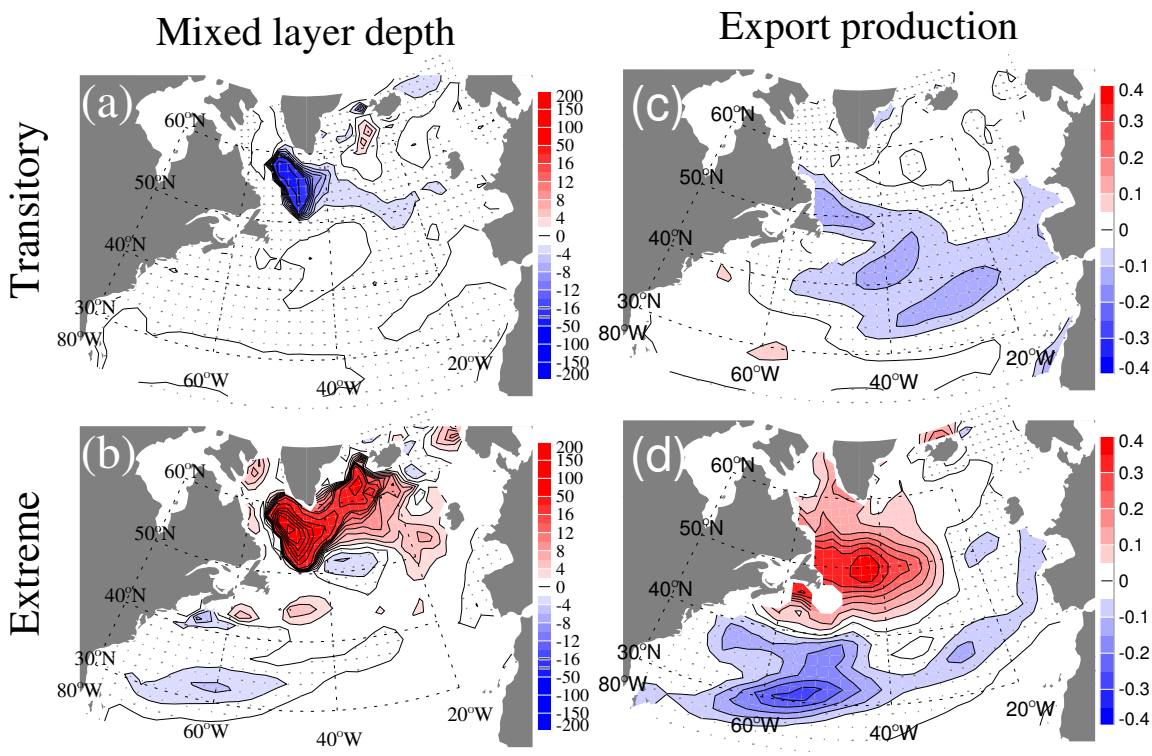

Fig. 16. Decadal mode anomalies of variations in mixed layer depth in m for the **(a)** transitory and **(b)** extreme phases as well as corresponding anomalies of export production in mol C m^{-2} $year^{-1}$ for the **(c)** transitory and **(d)** extreme phases.

Our analysis did identify delays in the air-sea CO_2 flux relative to climate forcing, with maximum correlation when the flux lags the climate forcing by 1 and 3 years. The 1-year lag may be due to the roughly 1-year equilibration time required for perturbations in atmospheric CO_2 to mix throughout the mixed layer (Broecker and Peng, 1974). Lags of up to 3 years have been documented previously in regard to interior ocean dynamics (Häkkinen, 1999; Gulev et al., 2003). In terms of air-sea CO_2 flux, our qualitative pattern matching suggests that such lags may be caused by export production linked with circulation-driven control factors. Evidence already exists that lateral advective processes partially control air-sea CO_2 flux in both the subtropical and subpolar gyres based on a Lagrangian model of mixed layer DIC content (Follows and Williams, 2004). Furthermore, lateral advection from higher latitude mode waters retains a signature of thermocline nutrient anomalies that is delivered to the subtropics (Palter et al., 2005). For subpolar air-sea CO_2 fluxes, lags may derive from advection within spatially heterogeneous tracer fields that stem in part from competition between entrainment and net carbon export production. Overall, the timescale for mixed layer DIC to equilibrate with the atmosphere (∼1 year) would increase when lower frequency oscillations due to lateral advection become important. Consequently, air-sea CO_2 flux variability would also be affected.

Further insight into these lags also comes from our linear decomposition of the basic formula for the air-sea CO_2 flux. At interannual timescales, the $\overline{Kg}\cdot\Delta pCO_2'$ term is mostly responsible for the lag between the climate forcing and the basin-wide air-sea CO_2 flux. This term reflects ocean processes, which is consistent with our previous discussion concerning these lags being driven by advection of anomalies of biogeochemically relevant tracers. A more quantitative, process-oriented study will be needed to better resolve the mechanisms responsible for the lags in the air-sea CO_2 flux relative to the climate forcing.

5 Conclusions

With an OGCM coupled to a biogeochemical model forced by 55 years of NCEP reanalysis winds, we made preindustrial and industrial-era simulations to study the variability of air-sea CO_2 fluxes in the North Atlantic. A basic lag-correlation analysis between the NAO and the air-sea CO_2 flux reveals complex spatiotemporal structure that cannot be resolved with traditional methods, such as EOF analysis. Thus we used MSSA to analyse interannual-to-decadal variability of climate and biogeochemical variables because it accounts, simultaneously, for temporal as well as spatial variability among a suite a variables.

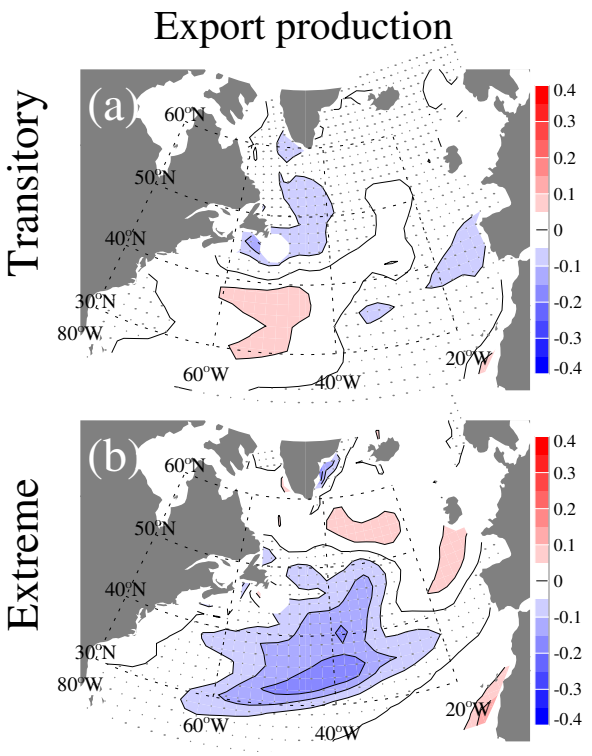

Fig. 17. The 5–7 year interannual mode anomalies of export production in mol C m^{-2} year^{-1} for the **(a)** transitory and **(b)** extreme phases.

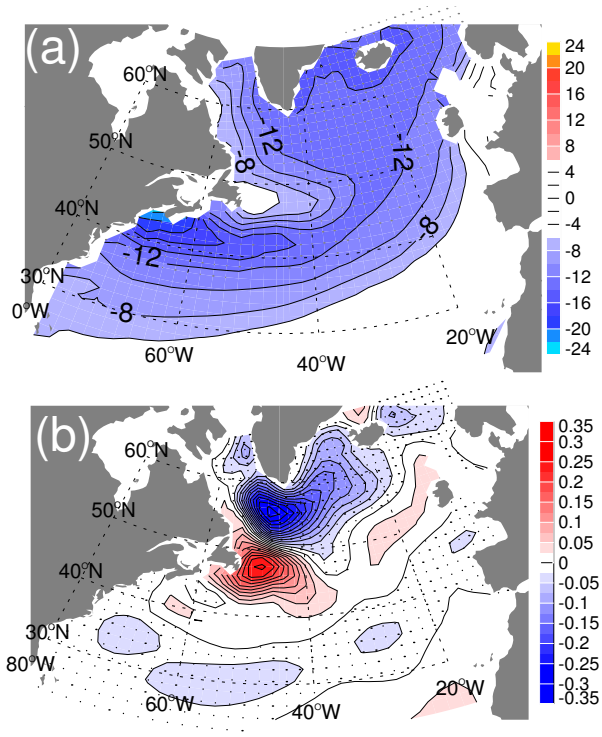

Fig. 18. **(a)** Historical minus preindustrial $\overline{\Delta pCO_2}$ (ppm) and **(b)** decadal variability for the extreme phase of the air-sea CO_2 flux as in Fig. 9d but for the control (preindustrial) simulation (mol C m^{-2} year^{-1}). The overall negative change in $\overline{\Delta pCO_2}$ from the preindustrial run to the historical run is responsible for a reinforcement of the $-Kg'\cdot\overline{\Delta pCO_2}$ term of Fig. 14d during an extreme phase. This change represents a very small negative contribution in the subtropical gyre and a more pronounced positive contribution in the subpolar region. Therefore, during an extreme phase, the area-integrated positive anomaly of (b) is increased from the preindustrial to the historical case of Fig. 9d.

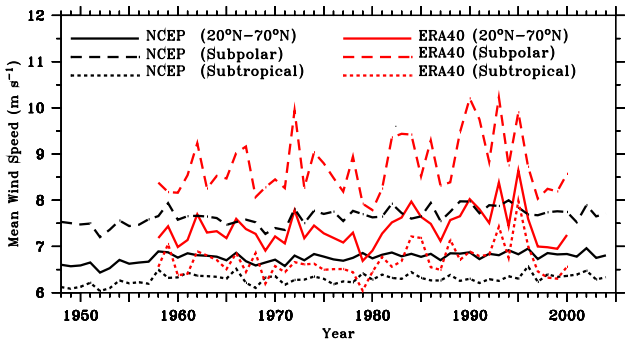

Fig. 19. Time series of annual mean 10-m wind speeds from NCEP and ERA40 reanalyses for area-weighted regional averages over the subtropical (20° N–45° N), the subpolar (45° N–70° N), and the entire North Atlantic (20° N–70° N).

Our MSSA analysis of SST and wind speed reveals structures and spectral properties that are well known, being characteristic of interannual-to-decadal climate variability over the North Atlantic and of the NAO in particular. These modes represent spatiotemporally coherent oscillations and explain 25% of the total variance; the remaining variability is explained by climate-related trends and noise. Variability of subtropical air-sea CO_2 fluxes is roughly similar at all frequencies (interannual to decadal), whereas in the subpolar gyre there are substantial differences between frequencies. Overall, we found that high and low anomalies extend throughout the North Atlantic and partially cancel one another, thereby damping total basin-wide air-sea CO_2 fluxes. Thus it is not reasonable to assume that variability in the subtropical gyre, namely at BATS, is representative of that in the intergyre and subpolar gyre, neither at interannual nor decadal timescales.

In addition, we found that decadal variability of the air-sea CO_2 flux is larger than interannual variability and is likely to grow in importance with time. Decadal variability increases with increasing atmospheric CO_2 because the $Kg'\cdot\overline{\Delta pCO_2}$ term increases in magnitude and it does so with large uniform anomalies in the north. The resulting effect becomes evident by comparing simulations with preindustrial and modern levels of CO_2. Increases in atmospheric CO_2 have enhanced decadal variability of the air-sea CO_2 flux in the North Atlantic by 30%. This geochemical enhancement of variability

is distinct from changes in variability that will develop due to future changes in climate. Therefore, decadal variability in North Atlantic air-sea CO_2 fluxes could well become relatively more important in a higher CO_2 world.

In the future, it would be useful to use MSSA to quantify contributions of individual terms to the air-sea CO_2 flux as well as to the DIC and alkalinity tracer-transport and source-minus-sink equations integrated over the mixed layer.

Appendix A

The Multichannel Singular Spectrum Analysis (MSSA)

The formalism used here for MSSA is inspired from Plaut and Vautard (1994). MSSA is a temporal extension of the so called Principal Component Analysis (PCA, Weare and Nasstrom (1982); Preisendorfer (1988)) also known as Empirical Orthogonal Functions (EOF) decomposition. PCA decomposes a space-time field into stationary EOF maps and associated scalar time series (principal component, PC). MSSA adds a temporal dimension to EOFs. Alternatively, MSSA can be understood as the multivariate version of the Singular Spectrum Analysis (SSA, Broomhead and King (1986); Vautard and Ghil (1989)). SSA is similar to PCA, except that associated EOFs are not spatial but purely temporal.

More specifically, let us consider a spatiotemporal field in a discrete environment $\{\mathbf{X}_{\ell i}\}$, ℓ. Here ℓ $(1\leq\ell\leq L)$ and i $(1\leq i\leq N)$ are the spatial and temporal indices, respectively. The PCA decomposition $\{a^k\}$ of this field, based only on orthonormal spatial EOFs $\{\mathbf{E}^k\}$ is expressed by

$$\mathbf{X}_{\ell i} = \sum_{k=1}^{L} a_i^k \mathbf{E}_\ell^k \ . \tag{A1}$$

Conversely, the decomposition based only on using orthonormal temporal EOFs of a scalar time series using SSA is

$$\mathbf{x}_{i+j} = \sum_{k=1}^{M} a_i^k \mathbf{E}_j^k \ , \tag{A2}$$

where j is the temporal lag index and M is the temporal window width parameter. Combining these two decompositions results in an MSSA decomposition:

$$\mathbf{X}_{\ell i+j} = \sum_{k=1}^{L} a_i^k \mathbf{E}_{\ell j}^k \ . \tag{A3}$$

where the space-time EOFs $\{\mathbf{E}_{\ell j}^k\}$ $(1\leq j\leq M)$ are the eigenvectors of the block-Toeplitz cross-covariance matrix $\mathbf{T}$ of $\mathbf{X}$.

$$\mathbf{T}\,\mathbf{E} = \Lambda\mathbf{E}\ , \tag{A4}$$

with Λ being the eigenvalues of $\mathbf{T}$.

$$(\mathbf{T}_{\ell\ell'})_{jj'} = \frac{1}{N-|j-j'|} \sum_{i=1}^{N-|j-j'|} \mathbf{X}_{\ell i}\mathbf{X}_{\ell' i+j-j'} \tag{A5}$$

where the primes refer to delayed indices. $(\mathbf{T}_{\ell\ell'})_{jj'}$ is the $j-j'$ lag covariance of $\mathbf{X}$ between spatial points ℓ and ℓ'.

Spatiotemporal oscillations are identified as pairs of modes (Plaut and Vautard, 1994; Vautard and Ghil, 1989). Each mode can be reconstructed following the classical EOF decomposition by suitably multiplying its space-time EOF by its PC. For the k-th mode, its associated reconstructed component is expressed by

$$\mathbf{X}_{\ell i}^k = \frac{1}{M}\sum_{i=1}^{M} a_{i-j}^k \mathbf{E}_{\ell j}^k \ , \tag{A6}$$

with $M\leq i\leq N-M+1$, and different approaches can be used for the boundary conditions (when $1\leq i\leq M-1$ and $N-M+1\leq i\leq N$, Broomhead and King (1986); Plaut and Vautard (1994)). Since a reconstructed component is only a part of the original field $\mathbf{X}_{\ell i}$, its dimensions are exactly the same, and the sum of all these components is equal to $\mathbf{X}_{\ell i}$. In this way, the signal associated with an oscillation can be extracted by summing the reconstruction of the two associated modes (for example $\mathbf{X}_{\ell i}^k+\mathbf{X}_{\ell i}^{k+1}$ for the pair $(k,\ k+1)$). In this paper, we use the term "oscillations" to refer to such reconstructions.

Acknowledgements. We thank G. Madec for discussions and P. Monfray for helping to initiate this project. This study was supported by the European Union 5th Framework NOCES project (Contract No. EVK2-CT-2001-00134) as well as the 6th Framework CARBOOCEAN project (Contract number 511176 (GOCE)). Computations were made at the French CNRS (IDRIS) and CEA (CCRT) supercomputing centres.

Edited by: M. Tomczak

References

Aumont, O. and Bopp, L.: Globalizing results from ocean in situ iron fertilization studies, Global Biogeochem. Cycles, 20, GB2017, doi:10.1029/2005GB002591, 2006.

Baker, D. F., Law, R. M., Gurney, K. R., Rayner, P., Peylin, P., Denning, A. S., Bousquet, P., Bruhwiler, L., Chen, Y.-H., Ciais, P., Fung, I. Y., Heimann, M., John, J., Maki, T., Maksyutov, S., Masarie, K., Prather, M., Pak, B., Taguchi, S., and Zhu, Z.: TransCom 3 inversion intercomparison: Impact of transport model errors on the interannual variability of regional CO_2 fluxes, 1988–2003, Global Biogeochem. Cycles, 20, GB1002, doi:10.1029/2004GB002439, 2006.

Bates, N.: Interannual variability of oceanic CO_2 and biogeochemical properties in the Western North Atlantic subtropical gyre, Deep-Sea Res. II, 48, 1507–1528, 2001.

Beckman, A. and Doscher, R.: A method for improved representation of dense water spreading over topography in geopotential-coordinate models, J. Phys. Oceanogr., 27, 581–591, 1997.

Blanke, B. and Delecluse, P.: Low frequency variability of the tropical Atlantic ocean simulated by a general circulation model with two different mixed layer physics, J. Phys. Oceanogr., 23, 1363–1388, 1993.

Blanke, B., Arhan, M., Lazar, A., and Prévost, G.: A Lagrangian numerical investigation of the origins and fates of the salinity maximum water in the Atlantic, J. Geophys. Res. (Oceans), 107, 3163, doi:10.1029/2002JC001318, 2005.

Bopp, L., Kohfeld, K. E., Quéré, C. L., and Aumont, O.: Dust impact on marine biota and atmospheric pCO_2 during glacial periods, Paleoceanogr., 18(2), 1046, doi:10.1029/2002PA000810, 2003.

Bopp, L., Aumont, O., Cadule, P., Alvain, S., and Gehlen, M.: Response of diatoms distribution to global warming and potential implications: A global model study, Geophys. Res. Lett., 32, L19606, doi:10.1029/2005GL023653, 2005.

Bousquet, P., Peylin, P., Ciais, P., Le Quéré, C., Friedlingstein, P., and Tans, P.: Regional changes in carbon dioxide fluxes of land and oceans since 1980, Science, 290, 1342–1346, 2000.

Boyer, T. P., Levitus, S., Antonov, J. I., Conkright, M. E., O'Brien, T. D., and Stephens, C.: World Ocean Atlas 1998 Vol. 4, NOAA Atlas NESDIS 30, 166 pp., 1998.

Brix, H., Gruber, N., and Keeling, C. D.: Interannual variability of the upper ocean carbon cycle at station ALOHA near Hawaii, Global Biogeochem. Cycles, 18, GB4019, doi:10.1029/2004GB002245, 2004.

Broecker, W. S. and Peng, T. H.: Gas exchange rates between air and sea, Tellus, 26, 21–35, 1974.

Broomhead, D. S. and King, G. P.: Extracting qualitative dynamics from experimental data, Physica D, 20, 217–236, 1986.

Czaja, A., Robertson, A. W., and Huck, T.: The role of the Ocean-Atmosphere Coupling Affecting the North Atlantic Variability, in: The North Atlantic Oscillation, edited by: Hurrell, J., Kushnir, Y., Ottersen, G., and Visbeck, M., Geophysical Monograph Series, 134, 147–172, American Geophysical Union, 2003.

Da Costa, E. and de Verdière, A. C.: The 7.7-year North Atlantic Oscillation, Quart. J. Roy. Meteorol. Soc., 128, 797–818, 2002.

Da Costa, E. and Vautard, R.: A qualitatively realistic low-order model of the extratropical low frequency variability built from long records of potential vorticity, J. Atmos. Sci., 55, 1064–1084, 1997.

Deser, C., Walsh, J. E., and Timlin, M. S.: Arctic Sea Ice Variability in the Context of Recent Atmospheric Circulation Trends, J. Climate, 13, 617–633, 2000.

Dutkiewicz, S., Follows, M., Marshall, J., and Gregg, W. W.: Interannual variability of phytoplankton abundances in the North Atlantic, Deep Sea Res. II, 48, 2323–2344, 2001.

Follows, M. and Williams, R.: The Ocean Carbon Cycle and Climate, chap. Mechanisms controlling the air-sea flux of CO2 in the North Atlantic, NATO-ASI volume, Kluwer, edited by: Follows, M. J. and Oguz, T., 2004.

Gent, P. R. and McWilliams, J. C.: Isopycnal mixing in ocean circulation models, J. Phys. Oceanogr., 20, 150–155, 1990.

Griffies, S. M., Böning, C., Bryan, F. O., Chassignet, E. P., Gerdes, R., Hasumi, H., Hirst, A., Treguier, A. M., and Webb, D.: Developments in ocean climate modelling, Ocean Modelling, 2, 123–192, 2001.

Gruber, N., Bates, N., and Keeling, C. D.: Interannual variability in the North Atlantic carbon sink, Science, 298, 2374–2378, 2002.

Gulev, S. K., Barnier, B., Knochel, H., Molines, J.-M., and Cottet, M.: Water mass transformation in the North Atlantic and its impact on the meridional circulation: Insights from an ocean model forced by NCEP-NCAR reanalysis surface fluxes, J. Climate, 16, 3085–3110, 2003.

Häkkinen, S.: Variability in the simulated meridional heat transport in the North Atlantic for the period 1951–1993, J. Geophys. Res., 104(C5), 10 991–11 007, doi:10.1029/1999JC900034, 1999.

Hasselmann, K.: PIPs and POPs: The reduction of complex dynamical systems using Principal Interaction and Oscillation patterns analysis, J. Geophys. Res., 93(D9), 11 015–11 021, 1988.

Hurrell, J., Kushnir, Y., Ottersen, G., and Visbeck, M. (Eds.): The North Atlantic Oscillation: Climate Significance and Environmental Impact, Geophysical Monograph Series, American Geophysical Union, vol. 134, 2003a.

Hurrell, J., Kushnir, Y., Ottersen, G., and Visbeck, M.: An Overview of the North Atlantic Oscillation, in: The North Atlantic Oscillation, edited by: Hurrell, J., Kushnir, Y., Ottersen, G., and Visbeck, M., Geophysical Monograph Series, 134, 1–36, American Geophysical Union, 2003b.

Jackett, D. R. and McDougall, T. J.: Minimal adjustment of hydrographic data to achieve static stability, J. Atmos. Oceanic Technol., 12, 381–389, 1995.

Jones, P. D., Osborn, T. J., and Briffa, K. R.: Pressure-Based Measures of the North Atlantic Oscillation (NAO): A Comparison an Assessment of Changes in the Strength of the NAO and in Its Influence on Surface Climate Parameters, in: The North Atlantic Oscillation, edited by: Hurrell, J., Kushnir, Y., Ottersen, G., and Visbeck, M., Geophysical Monograph Series, 134, 51–62, American Geophysical Union, 2003.

Joyce, T. M., Deser, C., and Spall, M. A.: The relation between decadal variability of subtropical mode water and the North Atlantic Oscillation, J. Climate, 13, 2550–2569, 2000.

Kalnay, E., Kanamitsu, M., Kistler, R., Collins, W., Deaven, D., Iredell, L. G. M., Saha, S., White, G., Woollen, J., Zhu, Y., Leetmaa, A., Reynolds, R., Chelliah, M., Ebisuzaki, W., Higgins, W., Janowiak, J., Mo, K. C., Ropelewski, C., Wang, J., Jenne, R., and Joseph, D.: The NCEP/NCAR 40-year reanalysis project, Bull. Amer. Meteorol. Soc., 77, 437–471, 1996.

Le Quéré, C., Orr, J. C., Monfray, P., Aumont, O., and Madec, G.: Interannual variability of the oceanic sink of CO_2 from 1979 through 1997, Global Biogeochem. Cycles, 14, 1247–1266, 2000.

Le Quéré, C., Aumont, O., Bopp, L., Bousquet, P., Ciais, P., Francey, R., Heimann, R., Kheshgi, H., Peylin, P., Piper, S., Prentice, I. C., and Rayner, P. J.: Two decades of ocean CO2 sink and variability, Tellus, 55, 649–656, 2003a.

Le Quéré, C., Aumont, O., Monfray, P., and Orr, J.: Propagation of climatic events on ocean stratification, marine biology, and CO2: Case studies over the 1979–1999 period, J. Geophys. Res., 108(C12), 1479, doi:10.1029/2003GL016867, 2003b.

Lengaigne, M., Boulanger, J.-P., Menkes, C., Masson, S., Madec, G., and Delecluse, P.: Ocean response to the March 1997 Westerly Wind Event, J. Geophys. Res., 107(C12), 8015, doi:10.1029/2001JC000841, 2002.

Lu, J. and Greatbatch, R. J.: The changing relationship between the NAO and northern hemisphere climate variability, Geophys. Res. Lett., 29, 2002.

Madec, G., Delecluse, P., Imbard, M., and Levy, C.: OPA version 8.1 Ocean General Circulation Model Reference Manual, Note du pôle de modélisation, 11, pp. 91, 1998.

Mahadevan, A., Lévy, M., and Mémery, L.: Mesoscale variability of sea surface pCO2: What does it respond to?, Global

Biogeochem. Cycles, 18, GB1017, doi:10.1029/2003GB002102, 2004.

Maltrud, M. E. and McClean, J. L.: An eddy resolving global 1/10° ocean simulation, Ocean Modelling, 8, 31–54, 2005.

Marsh, R.: Recent variability of the North Atlantic thermohaline circulation inferred from surface heat and freshwater fluxes, J. Climate, 13, 3239–3260, 2000.

McGillicuddy Jr., D. J., Johnson, R., Siegel, D. A., Michaels, A. F., Bates, N. R., and Knap, A. H.: Mesoscale variations of biogeochemical properties in the Sargasso Sea, J. Geophys. Res., 104, 13 381–13 394, 1999.

McKinley, G., Rodenbeck, C., Gloor, M., Houweling, S., and Heimann, M.: Pacific dominance to global air-sea CO2 flux variability: A novel atmospheric inversion agrees with ocean models, Geophys. Res. Lett., 31, L22308, doi:10.1029/2004GL021069, 2004a.

McKinley, G. A., Follows, M. J., and Marshall, J.: Mechanisms of air-sea CO2 flux variability in the equatorial Pacific and the North Atlantic, Global Biogeochem. Cycles, 18, GB2011, doi:10.1029/2003GB002179, 2004b.

Moron, V., Vautard, R., and Ghil, M.: Trends, decadal and interannual variability in global sea surface temperature fields, Clim. Dyn., 14, 545–569, 1998.

Oschlies, A.: NAO-induced long-term changes in nutrient supply to the surface waters of the North Atlantic, Geophys. Res. Lett., 28, 1751–1757, 2001.

Palter, J. B., Lozier, M. S., and Barber, R. T.: The effect of advection on the nutrient reservoir in the North Atlantic subtropical gyre, Nature, 437, 687–692, 2005.

Patra, P., Maksyutov, S., Ishizawa, M., Nakazawa, T., and Takahashi, T.: Interannual and decadal changes in the sea-air CO2 flux from atmospheric CO2 inverse modelling, Global Biogeochem. Cycles, 19, BGC4013, doi:10.1029/2004GB002257, 2005.

Peylin, P., Bousquet, P., Quéré, C. L., Sitch, S., Friedlingstein, P., McKinley, G., Gruber, N., Rayner, P., and Ciais, P.: Interannual CO2 fluxes as deduced by inverse modeling of atmospheric CO2 and by models of the ocean and the land carbon cycle, Global Biogeochem. Cycles, 19, GB1011, doi:10.1029/2003GB002214, 2005.

Plaut, G. and Vautard, R.: Spells of low-frequency oscillations and weather regimes in the northern hemisphere, J. Atmos. Sci., 2, 210–236, 1994.

Preisendorfer, R.: Principal Component Analysis in Meteorology and Oceanography, Elsevier Sci., pp. 426, 1988.

Rodenbeck, C., Houweling, S., Gloor, M., and Heimann, M.: CO_2 flux history 1982–2001 inferred from atmospheric data using a global inversion of atmospheric transport, Atmos. Chem. Phys., 3, 1919–1964, 2003, http://www.atmos-chem-phys.net/3/1919/2003/.

Rodgers, K. B., Aumont, O., Madec, G., Menkes, C., Blanke, B., Monfray, P., Orr, J. C., and Schrag, D. P.: Radiocarbon as a thermocline proxy for the eastern equatorial Pacific, Geophys. Res. Lett., 31, L14 314, doi:10.1029/2004GL019764, 2004.

Roullet, G. and Madec, G.: Salt conservation, free surface and varying volume: a new formulation for Ocean GCMs, J. Geophys. Res., 105, 23 927–23 942, 2000.

Smith, S. R., Legler, D. M., and Verzone, K. V.: Quantifying uncertainties in NCEP Reanalyses using high-quality research vessel observations., J. Climate, 14, 4062–4072, 2001.

Takahashi, T., Sutherland, S. C., Sweeney, C., Poisson, A., Metzl, N., Tilbrook, B., Bates, N., Wanninkhof, R., Feely, R. A., Sabine, C., Olafsson, J., and Nojiri, Y.: Global sea-air CO2 flux based on climatological surface ocean pCO2, and seasonal biological and temperature effects, Deep Sea Res. II, 49, 1601–1622, 2002.

Taylor, K. E.: Summarizing multiple aspects of model performance in single diagram, J. Geophys. Res., 106, 7183–7192, 2001.

Timmermann, R., Goosse, H., Madec, G., Fichefet, T., Ethe, C., and Dulière, V.: On the representation of high latitude processes in the ORCA-LIM global coupled sea ice ocean model, Ocean Modelling, 8, 175–201, 2005.

van der Avoird, E.: Low-frequency variability in the coupled ocean-atmosphere system at midlatitudes, Ph.D. thesis, Utrecht Univ., 112 pp., 2002.

Vautard, R. and Ghil, M.: Singular Spectrum Analysis in nonlinear dynamics,with application to paleoclimatic time series, Physica D, 35, 395–424, 1989.

Visbeck, M., Chassignet, E., Curry, R., Delworth, T., Dickson, B., and Krahmann, G.: The ocean's response to North Atlantic Oscillation variability, in: The North Atlantic Oscillation, edited by: Hurrell, J., Kushnir, Y., Ottersen, G., and Visbeck, M., Geophysical Monograph Series, 134, 113–146, American Geophysical Union, 2003.

Waliser, D. E., Shi, Z., Lanzante, J. R., and Oort, A. H.: The Hadley circulation: Assessing NCEP/NCAR reanalysis and sparse in-situ estimates, Clim. Dyn., 15, 719–735, 1999.

Weare, B. C. and Nasstrom, J. N.: Examples of extended empirical orthogonal fucntion analyses, Mon. Wea. Rev., 110, 481–485, 1982.

Wetzel, P., Winguth, A., and Maier-Reimer, E.: Sea-to-air CO_2 flux from 1948 to 2003: A model study, Global Biogeochem. Cycles, 19, GB2005, doi:10.1029/2004GB002 339, 2005.